

Chapter 3

Anisotropic Approach: Compact Star as Generalized Model

In this chapter, we have studied a new class of interior solutions that are singularity-free and useful for describing anisotropic compact star objects on spherically symmetric spacetime metric. We have considered metric potential $g_{rr} = B_0^2(r) = \frac{1}{(1-\frac{r^2}{R^2})^n}$, where $n > 2$. The various physical characteristics of the model are specifically examined for the pulsar PSRJ1903+327 with its current estimated data. According to analysis, every physical need for a physically admissible star is satisfied and all features are acceptable. Further, the stability of the model has been examined. Numerous physical characteristics are also highlighted in a graphical form.

3.1 Introduction

Strange stars and neutron stars are objects of interest for researchers in relativistic astrophysics. The research into relativistic stellar structure has been ongoing for more than a century. When a massive star explodes as a supernova, the phase transition between hadronic and strange quark matter may occur at a density higher than

the nuclear density as described by Bodmer [26]. The pressure inside these compact stars can be decomposed into two parts: the radial pressure p_r and tangential pressure p_\perp . The measure of anisotropy is defined as $8\pi\sqrt{3}S = p_r - p_\perp$. According to Geng *et. al.* [62], the intriguingly repeating fast radio bursts (FRBs) are caused by irregular fractional collapses of a strange star's crust caused by filling it with accretion materials from its low-mass companion. The anisotropy can occur on the existence of a solid core, the pressure of a type p-superfluid, a phase transition, a rotation, a magnetic field, a mixture of two fluids, etc. According to Kippenhahn *et. al.* [93], anisotropy in relativistic stars may be caused by the presence of a solid core or type 3A superfluid. Herrera and Santos [76] studied local anisotropy in self-gravitating systems. According to Weber [213], strong magnetic fields can also thought to be a source of anisotropic pressure inside a compact object. Dev and Gleiser [47], Dev and Gleiser[48], and Gleiser and Dev [63] have also discussed a model of an anisotropic star by assuming a special type of matter density.

Rahaman *et. al.* [166] studied the anisotropic model of Krori-Barua spacetime. A relativistic stellar model admitting a quadratic equation of state on Finch–Skea spacetime was proposed by Sharma and Ratanpal [179]. This was generalized by Pandya *et. al.* [149] on modified Finch Skea spacetime. Bhar [13] obtained a new model of an anisotropic superdense star that allows conformal motions in the presence of a quintessence field. This model well defined on Vaidya and Tikekar [211] spacetime and characterized by the parameter w_q with $-1 < w_q < -\frac{1}{3}$.

In connection with anisotropy, Maurya *et. al.* [101] studied an anisotropic analog of the Durgapal and Fuloria [53] solution. Maurya *et. al.* [108] investigated pressure anisotropy on a relativistic star. Maurya *et. al.* [109] did a comprehensive study of anisotropic compact stars by considering Buchdahl ansatz [29]. Dayanandan *et. al.* [43] presented a detailed analysis of the stability of anisotropic compact star

by considering Matese and Whitman [97] transformation. Dayanandan and Maurya [44] studied the charged compact star model for an anisotropic fluid distribution.

Recent studies have explored the presence of charge and anisotropy within the interior of stars. Das *et. al.* [42] studied an effect of anisotropy by considering metric potential $g_{rr} = (1 + \frac{r^2}{R^2})$ and described the exact solution. Maharaj and Takisa [127] studied charged anisotropic models using a quadratic equation of state. Sharma *et. al.* [180] presented closed-form solutions for an anisotropic matter distribution. Thirukkanesh *et. al.* [193] presented an algorithm to describe a relativistic self-gravitating fluid. Sunzu *et. al.* [181] studied charged anisotropic models using a linear equation of state. Bhar *et. al.* [22] proposed a compact stellar model in the presence of pressure anisotropy in modified Finch Skea spacetime using the ansatz $B_0^2(r) = (1 + \frac{r^2}{R^2})^n$.

3.2 Einstein field equations

To study the structure of compact and massive stars, we use Einstein's field equations

$$R_{\alpha\beta} - \frac{1}{2}Rg_{\alpha\beta} = \frac{8\pi G}{C^4}T_{\alpha\beta}. \quad (3.1)$$

Ricci tensor and energy-momentum tensor respectively denoted as $R_{\alpha\beta}$ and $T_{\alpha\beta}$, R is Ricci scalar and $g_{\alpha\beta}$ is metric tensor. The universal gravitational constant and speed of light are denoted as G and C respectively. We write the Schwarzschild coordinates for a 4-D spacetime with spherically symmetrical, the line element describing the interior spacetime $x^0 = t, x^1 = r, x^2 = \theta, x^3 = \phi$ as

$$ds^2 = -A_0^2(r)dt^2 + B_0^2(r)dr^2 + r^2(d\theta^2 + \sin^2\theta d\phi^2), \quad (3.2)$$

where $A_0(r)$ and $B_0(r)$, the gravitational potentials are yet to be determined. The energy-momentum tensor for anisotropic fluid distribution is given by

$$T_{\beta}^{\alpha} = (\rho + p_r)u^{\alpha}u_{\beta} + p_t g_{\beta}^{\alpha} + (p_r - p_t)\nu^{\alpha}\nu_{\beta}, \quad (3.3)$$

with $u^{\alpha}u_{\beta} = -\nu^{\alpha}\nu_{\beta} = 1$ and $u^{\alpha}\nu_{\beta} = 0$. Here the vector ν^{α} is the space-like vector and u_{α} is the fluid 4-velocity and it is orthogonal to ν^{α} , ρ represents the energy-density, p_r and p_{\perp} the fluid's radial and tangential pressures respectively.

The Einstein field equations governing the system are then obtained as (we set $G = c = 1$)

$$8\pi\rho = \left[\frac{1}{r^2} - \frac{1}{r^2 B_0^2} + \frac{2B_0'}{r B_0^3} \right], \quad (3.4)$$

$$8\pi p_r = \left[\frac{-1}{r^2} - \frac{1}{r^2 B_0^2} + \frac{2A_0'}{r A_0 B_0^2} \right], \quad (3.5)$$

$$8\pi p_{\perp} = \left[\frac{A_0''}{A_0 B_0^2} + \frac{A_0'}{r A_0 B_0^2} - \frac{B_0'}{r B_0^3} - \frac{A_0' B_0'}{A_0 B_0^3} \right]. \quad (3.6)$$

In equations (3.4)-(3.6), a 'prime' denotes differentiation with respect to r .

Making use of equation (3.5) and (3.6), we define the anisotropy as

$$8\pi\sqrt{3}S = 8\pi(p_{\perp} - p_r) = \left[\frac{A_0''}{A_0 B_0^2} - \frac{A_0'}{r A_0 B_0^2} - \frac{B_0'}{r B_0^3} - \frac{A_0' B_0'}{A_0 B_0^3} - \frac{1}{r^2 B_0^2} + \frac{1}{r^2} \right], \quad (3.7)$$

which must be zero at centre $r = 0$ of stellar object.

3.3 Generating Model

For solving the system (3.4)-(3.6), we have three equations with five unknowns $(\rho, p_r, p_\perp, A_0(r), B_0(r))$. We are free to select any two of them to complete this system. As a result, there are 10 possible ways to choose any two unknowns. According to studies Sharma and Ratanpal [179], Bhar and Ratanpal [15] select B^2 and p_r , Bhar and Rahaman [12] choose ρ along with p_r , Murad and Fatema [117] and Thirukkanesh *et. al.* [193] select A_0^2 with $8\pi\sqrt{3}S$ to model various compact stars. However, a very well-liked method is to select B_0^2 and an equation of state, which is a relation between matter density and radial pressure p_r . Numerous articles in this direction have been published like Sunzu *et. al.* [181], Bhar *et. al.* [14], Komathiraj and Maharaj [88], Bhar [11], Bhar [18], Bhar *et. al.* [16], Thomas and Pandya [200]. Das *et. al.* [39] have studied the metric potential in the form $B_0^2(r) = \frac{1}{(1-\frac{r^2}{R^2})^4}$ and have shown that it can represent a viable model of compact objects. Das *et. al.* [40] have studied the metric potential in the form $B_0^2(r) = \frac{1}{(1-\frac{r^2}{R^2})^6}$ and have shown that it can represent a viable model of compact star 4U1820-30.

To develop a physically reasonable model of the stellar configuration, we assume that the metric potential g_{rr} is expressed as B_0^2 given by

$$B_0^2(r) = \frac{1}{(1 - \frac{r^2}{R^2})^n}, \quad (3.8)$$

where $n > 2$ is a positive integer. By selecting this metric potential, the function $B_0^2(r)$ is guaranteed to be finite, continuous, and well-defined within the range of stellar interiors. Also $B_0^2(r) = 1$ for $r = 0$ ensures that it is finite at the centre. Again, the metric is regular at the centre since $(B_0^2(r))'_{r=0} = 0$.

With the choice of $B_0^2(r)$, equation (3.7) reduces to

$$8\pi\sqrt{3}S = \frac{1}{\left(1 - \frac{r^2}{R^2}\right)^{-n}} \left[\frac{A_0''}{A_0} - \frac{A_0'}{A_0} \left(\frac{1}{r} + \frac{n \frac{r^2}{R^2}}{\left(1 - \frac{r^2}{R^2}\right)} \right) - \frac{n}{\left(1 - \frac{r^2}{R^2}\right)} - \frac{1}{r^2} + \frac{\left(1 - \frac{r^2}{R^2}\right)^{-n}}{r^2} \right], \quad (3.9)$$

rearranging equation (3.9) we get,

$$\frac{A_0''}{A_0} - \frac{A_0'}{A_0} \left(\frac{1}{r} + \frac{n \frac{r^2}{R^2}}{\left(1 - \frac{r^2}{R^2}\right)} \right) - \frac{n}{\left(1 - \frac{r^2}{R^2}\right)} - \frac{1}{r^2} + \frac{\left(1 - \frac{r^2}{R^2}\right)^{-n}}{r^2} = 8\pi\sqrt{3}S \left(1 - \frac{r^2}{R^2}\right)^{-n}, \quad (3.10)$$

We choose $8\pi\sqrt{3}S$ to solve equation (3.10) as

$$8\pi\sqrt{3}S = \left(1 - \frac{r^2}{R^2}\right)^n \left(\frac{-n}{\left(1 - \frac{r^2}{R^2}\right)} - \frac{1}{r^2} + \frac{\left(1 - \frac{r^2}{R^2}\right)^{-n}}{r^2} \right). \quad (3.11)$$

The above choice for anisotropy is physically reasonable, as at the centre ($r = 0$) anisotropy vanishes as expected. Substituting equation (3.11) in (3.10), we obtain,

$$\frac{A_0''}{A_0} - \frac{A_0'}{A_0} \left(\frac{1}{r} + \frac{n \frac{r^2}{R^2}}{\left(1 - \frac{r^2}{R^2}\right)} \right) = 0. \quad (3.12)$$

We obtain a simple solution of the equation (3.12)

$$A_0(r) = \frac{C(R^2 - r^2)^{1 - \frac{n}{2}}}{n - 2} + D. \quad (3.13)$$

Where C and D are integration constants. The interior spacetime metric takes the form

$$ds^2 = - \left(\frac{C(R^2 - r^2)^{1 - \frac{n}{2}}}{n - 2} + D \right)^2 dt^2 + \frac{1}{\left(1 - \frac{r^2}{R^2}\right)^n} dr^2 + r^2(d\theta^2 + \sin^2\theta d\phi^2). \quad (3.14)$$

The matter density, radial pressure, and tangential pressure take the form,

$$8\pi\rho = -\frac{-1 + \left(1 - \frac{r^2}{R^2}\right)^n}{r^2} + \frac{2n \left(1 - \frac{r^2}{R^2}\right)^{-1-n}}{R^2}, \quad (3.15)$$

$$8\pi p_r = \frac{-1 + \left(1 - \frac{r^2}{R^2}\right)^n}{r^2} - \frac{2C(-2+n) \left(1 - \frac{r^2}{R^2}\right)^n}{C(r^2 - R^2) - D(-2+n)(-r^2 + R^2)^{n/2}}, \quad (3.16)$$

$$8\pi p_\perp = -\frac{\left(1 - \frac{r^2}{R^2}\right)^n (C(-4+n)(r^2 - R^2) + D(-2+n)n(-r^2 + R^2)^{n/2})}{(r^2 - R^2)(C(r^2 - R^2) - D(-2+n)(-r^2 + R^2)^{n/2})}, \quad (3.17)$$

where integration constants, will be determined using boundary conditions.

3.4 Exterior Spacetime and Boundary Conditions

At the boundary of the star $r = b$, we match the interior metric (3.14) with the Schwarzschild exterior spacetime metric.

$$ds^2 = -\left(1 - \frac{2M}{r}\right) dt^2 + \left(1 - \frac{2M}{r}\right)^{-1} dr^2 + r^2(d\theta^2 + \sin^2\theta d\phi^2), \quad (3.18)$$

which leads to

$$A_0^2(r = b) = \left(1 - \frac{2M}{b}\right), \quad (3.19)$$

$$B_0^2(r = b) = \left(1 - \frac{2M}{b}\right)^{-1}, \quad (3.20)$$

At the boundary of stars $p_r(r = b) = 0$ which gives,

$$R = \sqrt{\frac{b^2}{1 - \sqrt[n]{1 - \frac{2M}{b}}}}, \quad (3.21)$$

$$C = \frac{R^n \left(-1 + \left(1 - \frac{b^2}{R^2}\right)^n\right)}{-2b^2}, \quad (3.22)$$

$$D = \left(1 - \frac{b^2}{R^2}\right)^{n/2} + \frac{R^n \left(-1 + \left(1 - \frac{b^2}{R^2}\right)^n\right) (R^2 - b^2)^{1-\frac{n}{2}}}{2(n-2)b^2}, \quad (3.23)$$

when the values of C and D are substituted in p_r and p_\perp we obtain,

$$8\pi p_r = \frac{-1 + \left(1 - \frac{r^2}{R^2}\right)^n}{r^2} + \frac{\left(1 - \left(1 - \frac{b^2}{R^2}\right)^n\right) \left(1 - \frac{r^2}{R^2}\right)^n R^n (R^2 - r^2)^{-\frac{n}{2}}}{b^2 \left(\left(1 - \frac{r^2}{R^2}\right)^{n/2} + \frac{\left(-1 + \left(1 - \frac{b^2}{R^2}\right)^n\right) R^n (R^2 - b^2)^{1-\frac{n}{2}}}{2b^2(n-2)} - \frac{\left(-1 + \left(1 - \frac{b^2}{R^2}\right)^n\right) R^n (R^2 - r^2)^{1-\frac{n}{2}}}{2b^2(n-2)} \right)}, \quad (3.24)$$

$$8\pi p_\perp = 8\pi p_r + 8\pi\sqrt{3}S, \quad (3.25)$$

Table 3.1: The numerical values of the strong energy condition at centre as well as surface, Gravitational Redshift at surface, and Adiabatic Index at the surface for the compact star PSR J1903+327.

n	$\rho - \mathbf{pr} - 2\mathbf{p}_\perp(r=0)$ (MeV fm ⁻³)	$\rho - \mathbf{pr} - 2\mathbf{p}_\perp(r=b)$ (MeV fm ⁻³)	$\mathbf{Z}_{(r=b)}$ (Gravitational Redshift)	$\mathbf{\Gamma}_{(r=0)}$ (Adiabatic Index)
$n = 4$	377.861	346.899	0.44166	3.59
$n = 6$	418.23	330.826	0.44166	3.15
$n = 10$	451.728	318.434	0.44166	2.85
$n = 15$	468.892	312.388	0.44166	2.71
$n = 20$	477.58	309.402	0.44166	2.65
$n = 50$	493.40	304.089	0.44166	2.54
$n = 70$	496.439	303.085	0.44166	2.52

The next section contains a physical analysis.

Table 3.2: The numerical values of the $\frac{dp_r}{d\rho}$ at centre as well as a surface and $\frac{dp_\perp}{d\rho}$ at centre as well as surface for the compact star PSR J1903+327.

n	$\frac{dp_r}{d\rho} (r=0)$	$\frac{dp_\perp}{d\rho} (r=0)$	$\frac{dp_r}{d\rho} (r=b)$	$\frac{dp_\perp}{d\rho} (r=b)$	$(\nu_t^2 - \nu_r^2)_{(r=b)}$
$n = 4$	0.462272	0.262272	0.360596	0.19339	-0.1672
$n = 6$	0.3719	0.1719	0.3130	0.1517	-0.1613
$n = 10$	0.31227	0.1122	0.2806	0.1338	-0.1468
$n = 15$	0.2858	0.0858	0.2658	0.1236	-0.1434
$n = 20$	0.2733	0.0733	0.2587	0.1188	-0.1422
$n = 50$	0.2520	0.052	0.2465	0.1108	-0.1357
$n = 70$	0.2480	0.0480	0.2443	0.1093	-0.135

Table 3.3: The values of the curvature parameter R for the compact star PSR J1903+327 whose observed mass and radius is given by $1.66_{-0.021}^{+0.021}M_\odot$ and $9.438_{-0.03}^{+0.03}km$ respectively

Star	Estimated Mass M_\odot	Estimated Radius	n	R Km
<i>PSRJ1903 + 327</i>	1.66	9.438	$n = 4$	23.085
			$n = 6$	27.856
			$n = 10$	35.533
			$n = 15$	43.257
			$n = 20$	49.796
			$n = 50$	78.309
			$n = 70$	92.560

3.5 Physical Analysis

A physically acceptable stellar model should comply with the following conditions throughout its region of validity.

- (i) $\rho(r) \geq 0, \quad p_r(r) \geq 0, \quad p_\perp(r) \geq 0, \quad \text{for } 0 \leq r \leq R$
- (ii) $\frac{d\rho}{dr} \leq 0, \quad \frac{dp_r}{dr} \leq 0, \quad \frac{dp_\perp}{dr} \leq 0, \quad \text{for } 0 \leq r \leq R$
- (iii) $0 \leq \frac{dp_r}{d\rho} \leq 1, \quad 0 \leq \frac{dp_\perp}{d\rho} \leq 1, \quad \text{for } 0 \leq r \leq R$
- (iv) $\rho - p_r - 2p_\perp \geq 0, \quad \text{for } 0 \leq r \leq R$
- (v) $\Gamma > \frac{4}{3}, \quad \text{for } 0 \leq r \leq R$

The central density, central radial pressure and central tangential pressure in this

case are:

$$\begin{aligned}\rho(0) &= \frac{3n}{R^2}, \\ p_r(0) &= \frac{-n}{R^2} + \frac{2C(n-2)}{-C(R^2) - D(n-2)(R^2)^{\frac{n}{2}}}, \\ p_{\perp}(0) &= \frac{-n}{R^2} + \frac{2C(n-2)}{-C(R^2) - D(n-2)(R^2)^{\frac{n}{2}}}.\end{aligned}$$

Note that the density is always positive as R is a positive quantity. The radial pressure and tangential pressure at the centre are equal which means pressure anisotropy vanishes at the centre. The radial and tangential pressures at the centre will be non-negative if one chooses the model parameters satisfying the conditions $n > 2$.

3.5.1 Energy Conditions

The most crucial requirement for our model to be physically plausible, i.e. strong energy condition (SEC).

$$SEC : \rho - p_r - 2p_{\perp} \geq 0. \quad (3.26)$$

Table(3.1) shows the values of $\rho - p_r - 2p_{\perp}$ at a centre as well as the surface of the star.

3.5.2 Causality and Stability Conditions

(i) Causality condition:

In this model, the square of sound speed is less than 1 in the interior of the star, i.e., $0 \leq \frac{dp_r}{d\rho} \leq 1$, $0 \leq \frac{dp_{\perp}}{d\rho} \leq 1$ which has been shown graphically in the next section.

Table(3.2) shows the values of $\frac{dp_r}{d\rho}$ and $\frac{dp_{\perp}}{d\rho}$ at a centre as well as the surface of the star. Abreu *et. al.* [1] proposed that, for a possibly stable configuration, $v_{\perp}^2 - v_r^2 < 0$, the stability factor is negative, as can be seen in Table(3.2). With this, we conclude

that our model may be stable everywhere in the stellar interior.

(ii) Relativistic adiabatic index:

Bondi [24] investigated whether a Newtonian isotropic sphere will be in equilibrium for a specific stellar configuration if the adiabatic index $(\Gamma) > 4/3$ and it is adapted for a relativistic anisotropic fluid sphere. Based on these findings, it can be determined that an anisotropic star configuration's stability depends on the adiabatic index Γ by,

$$\begin{aligned} \Gamma_r &= \frac{\rho + p_r}{p_r} \frac{dp_r}{d\rho}, \\ &= \frac{2 \left(1 - \frac{r^2}{R^2}\right)^n \left(-\frac{n}{r^2 - R^2} - \frac{C(n-2)}{\Phi}\right)}{\frac{-1 + (1 - \frac{r^2}{R^2})^n}{r^2} - \frac{2C(n-2)(1 - \frac{r^2}{R^2})^n}{\Phi}} v_r^2. \end{aligned} \quad (3.27)$$

Adiabatic index indicates that the condition $\Gamma > \frac{4}{3}$ is satisfied in the region $0 \leq r \leq 9.438$. Table (3.1) shows the values of Γ at the centre of the star.

3.5.3 Gravitational Redshift

The gravitational redshift z_G should be monotonically decreasing towards the boundary of the star. The central redshift z_G and boundary redshift z_G must be positive and finite. That is,

$$z_G = \sqrt{\frac{1}{e^\nu}} - 1. \quad (3.28)$$

The gravitational redshifts z_G are shown in Table (3.1).

3.5.4 Stability under Three Forces

The equation can be used to describe the stability of our current model under three forces: gravity force, hydrostatic force and anisotropic force.

$$-\frac{M_G(r)(\rho + p_r)}{r^2} \frac{B}{A} - \frac{dp_r}{dr} + \frac{2}{r}(p_\perp - p_r) = 0, \quad (3.29)$$

The Tolman-Whittaker formula and Einstein's field equations may be used to calculate $M_G(r)$, which stands for the gravitational mass inside the radius r , and is defined by

$$M_G(r) = r^2 \frac{A'}{B}. \quad (3.30)$$

Equation (3.29) changes to,

$$F_g + F_h + F_a = 0, \quad (3.31)$$

$$F_g = -\frac{2C(n-2)r(1 - \frac{r^2}{R^2})^n(2C(n-1)(r^2 - R^2) - Dn(n-2)(R^2 - r^2)^{\frac{n}{2}})}{(r^2 - R^2)(\Phi)^2}, \quad (3.32)$$

$$F_h = -\frac{2(-1 + \frac{r^2}{R^2})^n}{r^3} - \frac{2n(1 - \frac{r^2}{R^2})^{n-1}}{rR^2} + \frac{4Cnr(n-2)(1 - \frac{r^2}{R^2})^{n-1}}{R^2(\Phi)^2} + \frac{2C(n-2)(1 - \frac{r^2}{R^2})^n(2Cr + Dnr(n-2)(R^2 - r^2)^{\frac{n-2}{2}})}{(\Phi)^2}, \quad (3.33)$$

$$F_a = \frac{2\left(r^2\left(1 - \left(1 - \frac{r^2}{R^2}\right)^n + \left(1 - \frac{r^2}{R^2}\right)^n\right) + \left(-1 + \left(1 - \frac{r^2}{R^2}\right)^n\right)R^2\right)}{r^5 - r^3R^2}, \quad (3.34)$$

where

$$\Phi = C(r^2 - R^2) - D(n-2)(R^2 - r^2)^{\frac{n}{2}}.$$

Fig.(3.11) shows the graphical representation of three distinct forces for the compact star PSR J1903+327 with 'n=10'. According to the graphs, the gravitational force is a net negative force that predominates in nature. Hydrostatic and anisotropic forces work together to balance this force and keep the system in equilibrium.

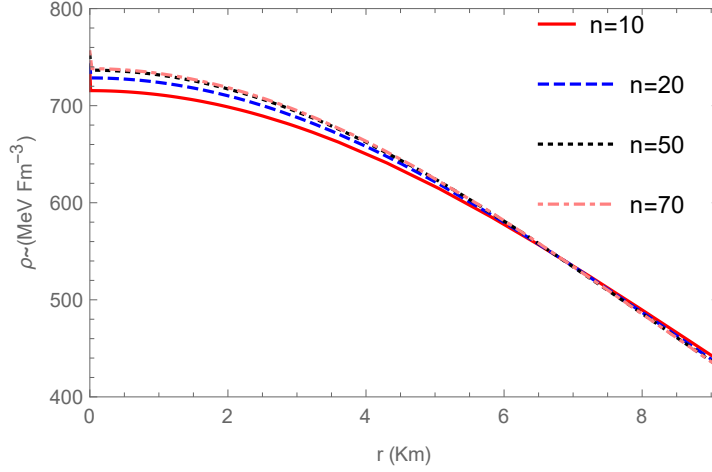


Figure 3.1: Variation of density (ρ) in MeV Fm^{-3} with respect to a radial coordinate r for a star PSR J1903+327 within the range $[0, 9.438]$ kms for different values of n .

3.6 Discussion

By assuming pressure anisotropy profile and a metric potential $B_0^2(r) = \frac{1}{(1 - \frac{r^2}{R^2})^n}$, that are physically plausible, the current work offers a new generalised model of compact stars. To set the values of the various constants, we compared our interior solution to the Schwarzschild exterior solution at the boundary $r = b$ of the star. The compact star PSR J1903+327 with mass and radius $M = 1.66M_\odot$ and $b = 9.438$ km respectively. we have studied the values of R , C , and D from the boundary conditions for various values of the dimensionless parameter "n". For the compact star PSR J1903+327, different values of "n" satisfy all physical plausibility conditions for matter density (ρ), radial pressure (p_r) and tangential pressure (p_\perp), square of sound speed of radial and tangential ($\frac{dp_r}{d\rho}$ and $\frac{dp_\perp}{d\rho}$), adiabatic Index (Γ), gravitational redshift (Z) and strong energy condition ($\rho - p_r - 2p_\perp$).

In Fig.(3.1) we have shown the variation of density for $0 \leq r \leq 9.438$. It is clear from the graph that the density is a decreasing function of r . In Fig.(3.2) and Fig.(3.3), we have shown the variation of radial and tangential pressures through-

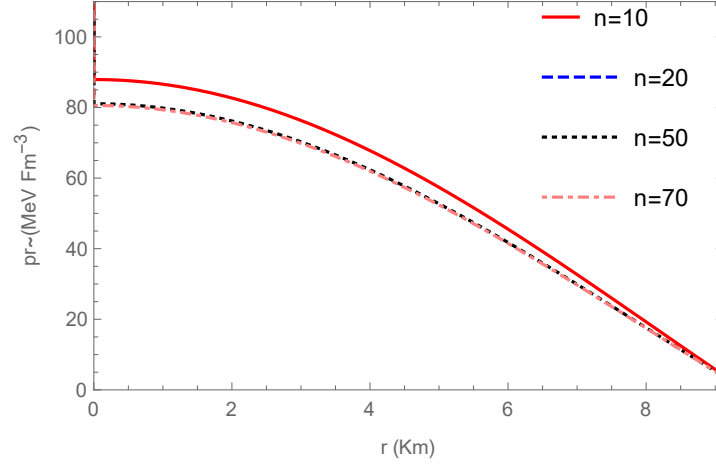


Figure 3.2: Variation of radial pressures (p_r) in MeV Fm^{-3} with respect to a radial coordinate r for a star PSR J1903+327 within the range $[0, 9.438]$ kms for different values of n .

out the star. It can be seen that both pressures are decreasing radially outwards. In Fig.(3.4) and Fig.(3.5), we have displayed the variation of $\frac{dp_r}{d\rho}$ and $\frac{dp_\perp}{d\rho}$ against r . Both quantities satisfy the restriction $0 < \frac{dp_r}{d\rho} < 1$ and $0 < \frac{dp_\perp}{d\rho} < 1$ indicating that the square of sound speed is less than the speed of light throughout the star. Fig.(3.6) shows anisotropy decreasing throughout the star. Fig.(3.7) shows the strong energy condition decreasing and positive throughout the distribution. For various values of ' n ', the profile of the adiabatic index (Γ_r) for our current model is shown in Fig(3.8). The graph shows that the radial adiabatic index profile is a monotonic increasing function of r and that $\Gamma = \frac{\rho + p_r}{p_r} \frac{dp_r}{d\rho} > \frac{4}{3}$ everywhere in the star arrangement, satisfying the stability requirement. The Gravitational redshifts z_G are shown in Fig.(3.9), which indicates the decreasing and finite at the surface as well as the boundary of the surface. Fig.(3.10) shows that $v_\perp^2 - v_r^2 < 0$ throughout the star. Fig.(3.11) shows the graphical representation of three distinct forces for the compact star PSR J1903+327. All the physically plausible conditions are satisfied throughout the distribution. Hence the model is suitable to describe PSR J1903+327.

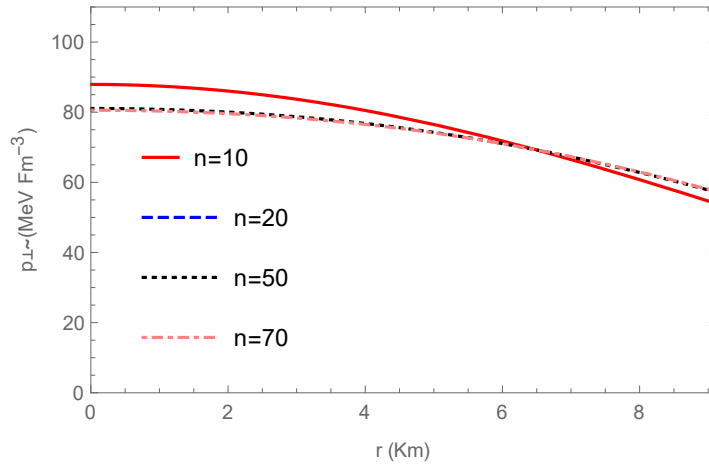


Figure 3.3: Variation of tangential pressures (p_{\perp}) in MeV Fm^{-3} with respect to a radial coordinate r for a star PSR J1903+327 within the range $[0, 9.438]$ kms for different values of n .

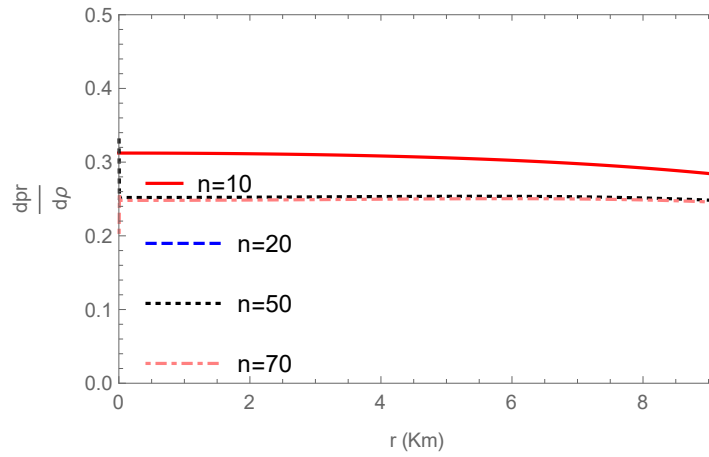


Figure 3.4: Variation of radial sound speed $\frac{dp_r}{d\rho}$ with respect to a radial coordinate r for a star PSR J1903+327 within the range $[0, 9.438]$ kms for different values of n .

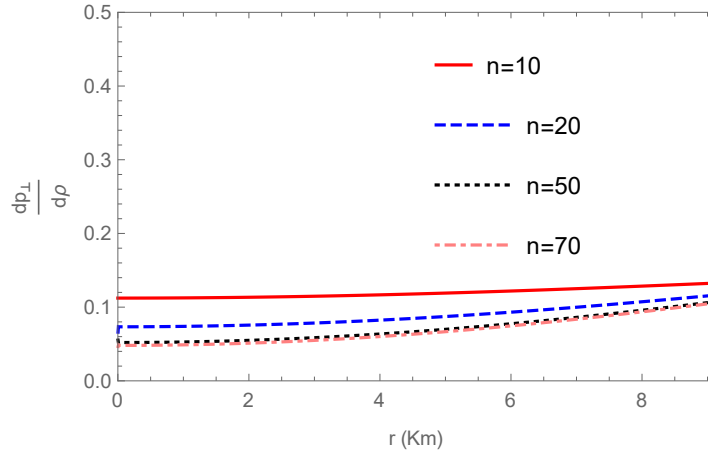


Figure 3.5: Variation of tangential sound speed $\frac{dp_{\perp}}{d\rho}$ with respect to a radial coordinate r for a star PSR J1903+327 within the range $[0, 9.438]$ kms for different values of n .

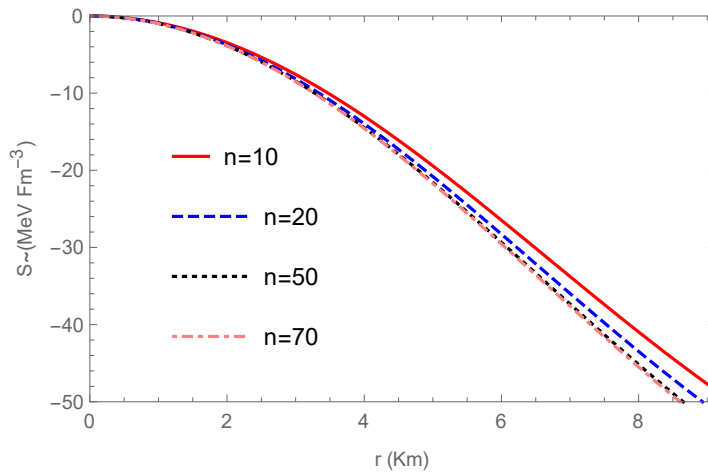


Figure 3.6: Variation of anisotropy $(8\pi\sqrt{3}S)$ in MeV Fm^{-3} with respect to a radial coordinate r for a star PSR J1903+327 within the range $[0, 9.438]$ kms for different values of n .

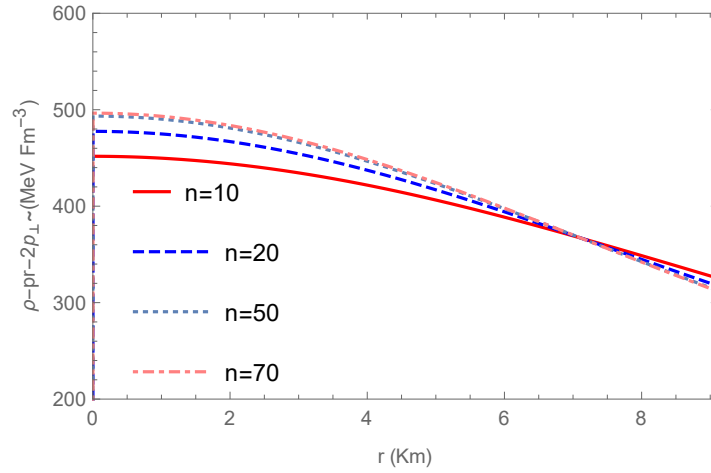


Figure 3.7: Variation of strong energy conditions ($\rho - p_r - 2p_\perp$) in MeV Fm^{-3} with respect to a radial coordinate r for a star PSR J1903+327 within the range $[0, 9.438]$ kms for different values of n .

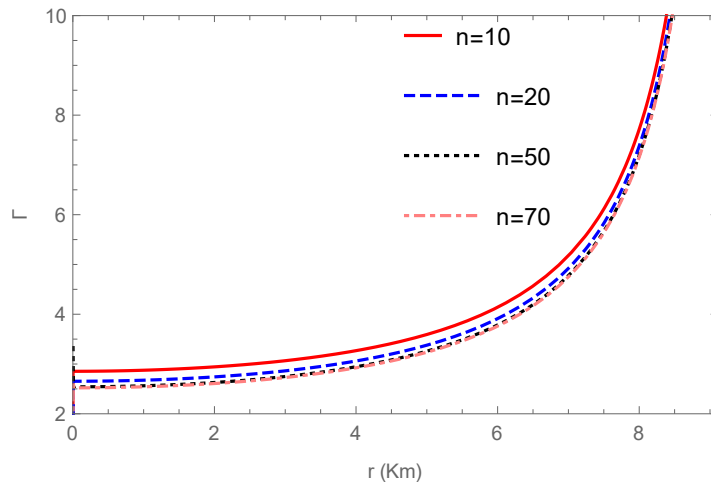


Figure 3.8: Variation of Adiabatic Index (Γ) with respect to a radial coordinate r for a star PSR J1903+327 within the range $[0, 9.438]$ kms for different values of n .

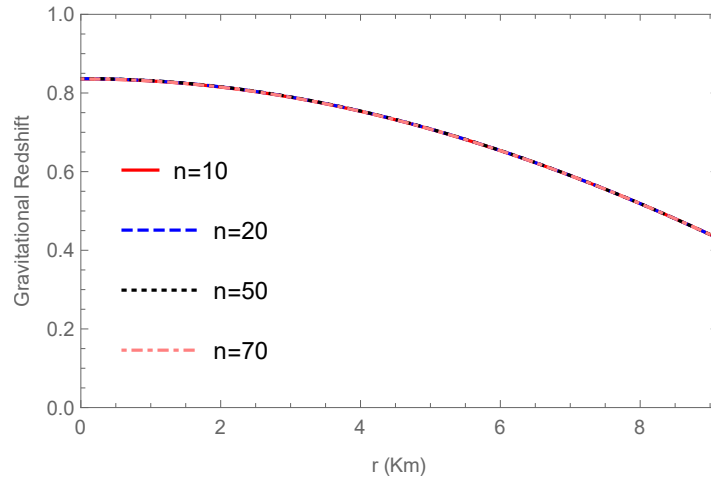


Figure 3.9: Variation of Gravitational Redshift (Z_G) with respect to a radial coordinate r for a star PSR J1903+327 within the range $[0,9.438]$ kms for different values of n .

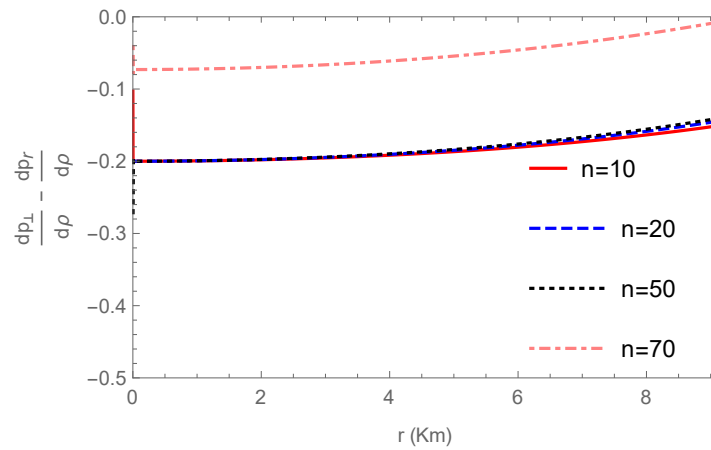


Figure 3.10: Variation of a stability expression $(\frac{dp_{\perp}}{d\rho} - \frac{dp_r}{d\rho})$ with respect to a radial coordinate r for a star PSR J1903+327 within the range $[0,9.438]$ kms for different values of n .

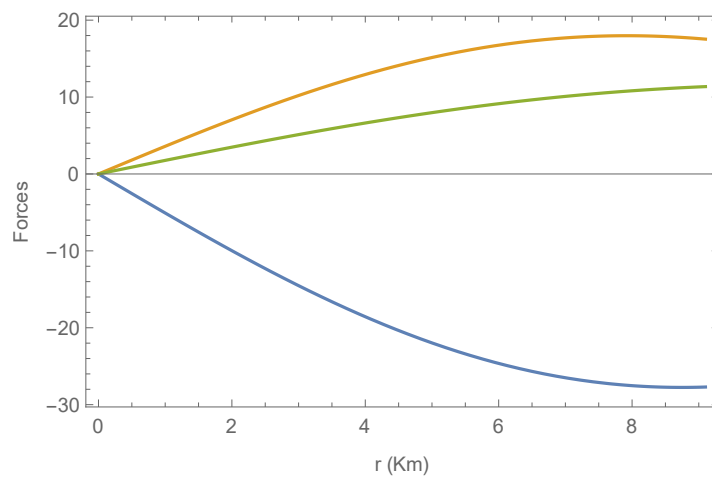


Figure 3.11: Variation of three forces Gravitational Force(Blue), Hydrostatic Force(Orange) and Anisotropic Force(Green) for the compact star PSR J1903+327.